ACS Biomaterials SCIENCE & ENGINEERING

Subscriber access provided by University of Kent

Characterization, Synthesis, and Modifications

Mesoporous phosphate-based glasses prepared via sol-gel

Daniela Carta, Farzad Foroutan, Benjamin Alexander Kyffin, Isaac Abrahams, Anna Corrias, Priyanka Gupta, Eirini G. Velliou, and Jonathan C. Knowles

ACS Biomater. Sci. Eng., **Just Accepted Manuscript** • DOI: 10.1021/acsbiomaterials.9b01896 • Publication Date (Web): 11 Feb 2020

Downloaded from pubs.acs.org on February 12, 2020

Just Accepted

"Just Accepted" manuscripts have been peer-reviewed and accepted for publication. They are posted online prior to technical editing, formatting for publication and author proofing. The American Chemical Society provides "Just Accepted" as a service to the research community to expedite the dissemination of scientific material as soon as possible after acceptance. "Just Accepted" manuscripts appear in full in PDF format accompanied by an HTML abstract. "Just Accepted" manuscripts have been fully peer reviewed, but should not be considered the official version of record. They are citable by the Digital Object Identifier (DOI®). "Just Accepted" is an optional service offered to authors. Therefore, the "Just Accepted" Web site may not include all articles that will be published in the journal. After a manuscript is technically edited and formatted, it will be removed from the "Just Accepted" Web site and published as an ASAP article. Note that technical editing may introduce minor changes to the manuscript text and/or graphics which could affect content, and all legal disclaimers and ethical guidelines that apply to the journal pertain. ACS cannot be held responsible for errors or consequences arising from the use of information contained in these "Just Accepted" manuscripts.

is published by the American Chemical Society. 1155 Sixteenth Street N.W., Washington, DC 20036

Published by American Chemical Society. Copyright © American Chemical Society. However, no copyright claim is made to original U.S. Government works, or works produced by employees of any Commonwealth realm Crown government in the course of their duties.

Mesoporous phosphate-based glasses prepared via sol-gel

Farzad Foroutan,[a] Benjamin A. Kyffin,[a] Isaac Abrahams,[b] Anna Corrias,[c] Priyanka Gupta,[d] Eirini Velliou,[d] Jonathan C. Knowles,[e,f,g,h] Daniela Carta[a,]*

[a] *Department of Chemistry, University of Surrey, GU2 7XH, Guildford, UK.*

[b] *Materials Research Institute, School of Biological and Chemical Sciences, Queen Mary, University of London, Mile End Road, London E1 4NS, UK.*

[c] *School of Physical Sciences, University of Kent, Canterbury, CT2 7NH, UK.*

[d] *Department of Chemical and Process Engineering, Bioprocess and Biochemical Engineering group (BioProChem), University of Surrey, Guildford, UK.*

[e] *Division of Biomaterials and Tissue Engineering, University College London, Eastman Dental Institute, 256 Gray's Inn Road, London WC1X 8LD, UK.*

[f] *The Discoveries Centre for Regenerative and Precision Medicine, UCL Campus, London, UK.*

[g] *Department of Nanobiomedical Science & BK21 PLUS NBM Global Research Center for Regenerative Medicine, Dankook University, Cheonan 31114, Republic of Korea.*

[h] *UCL Eastman-Korea Dental Medicine Innovation Centre, Dankook University, Cheonan 31114, Republic of Korea.*

**Corresponding author: Dr D. Carta, Department of Chemistry, University of Surrey, GU2 7XH, Guildford, UK. Email: d.carta@surrey.ac.uk*

ABSTRACT

In the present study, a mesoporous phosphate-based glass (MPG) in the P_2O_5-CaO-Na_2O system was synthesised, for the first time, using a combination of sol-gel chemistry and supramolecular templating. A comparison between the structural properties, bioactivity and biocompatibility of the MPG with a non-porous phosphate-based glass (PG) of analogous composition prepared via the same sol-gel synthesis method, but in the absence of a templating surfactant is also presented. Results indicate that the MPG has enhanced bioactivity and biocompatibility compared to the PG, despite having similar local structure and dissolution properties. In contrast to the PG, the MPG shows formation of hydroxyl carbonate apatite (HCA) on its surface after 24 hours of immersion in simulated body fluid. Moreover, MPG shows enhanced viability of Saos-2 osteosarcoma cells after 7 days of culturing. This suggests that textural properties (porosity and surface area) play a crucial role in the kinetics of HCA formation and in interaction with cells. Increased efficiency of drug loading and release over non-porous PG systems was proved using the antimicrobial tetracycline hydrochloride as a drug model. This study represents a significant advance in the field of mesoporous materials for drug delivery and bone tissue regeneration as it reports, for the first time, the synthesis, structural characterisation and biocompatibility of mesoporous calcium phosphate glasses.

Keywords: Mesoporous materials, sol-gel, phosphate glasses, bone regeneration, drug delivery.

1. INTRODUCTION

Mesoporous glasses for biomedical applications have gained increasing attention in the past years.[1, 2, 3] Their main characteristics are the presence of extended porosity with pores in the size range of 2-50 nm, high surface areas and high pore volumes, which make them ideal systems for controlled drug delivery and tissue regeneration applications. Introduction of mesoporosity into biomedical glasses i) enhances the interaction between the bioresorbable implant and physiological fluids; ii) facilitates the absorption and delivery of therapeutic molecules thanks to the open porous structure and homogeneity of pore sizes; iii) guarantees multifunctionality, by combining drug delivery and cell stimulation. To date, a significant amount of work has been performed on the synthesis of mesoporous silicate-based glasses mainly as drug delivery systems[4, 5] and for bone tissue regeneration applications.[6] It has been shown that mesopores can be loaded with high dosages of osteogenic agents and therapeutic molecules and that high surface areas enhance the bioactivity of silicate-based glasses.[7, 8] However, to date, there are no examples of mesoporous phosphate-based glasses (MPGs) reported in the literature. The synthesis of MPGs has been considered in a recent review as "*a significantly challenging area for future efforts*".[8] This is because the phophate-based glass network is more prone to collapsing and crystallisation than the silicate-based glasses under the processes required to obtain the mesoporous structure.[8] It has also to be noted that the synthesis of mesoporous oxides containing P and Ca is particularly challenging even in crystalline form.[9]

Phosphate-based glasses (PGs) have recently been presented as a promising new generation of biomaterials as alternatives to the silicate-based glasses. PGs can be defined as bioresorbable, as they are able to interact with the physiological fluids producing the desired biological response and simultaneously dissolve completely over time being eventually entirely replaced by regenerated hard or soft tissue.[10, 11]

In contrast,silicate-based glasses, have a very slow solubility and can only be used to manufacture long-term implants, which are susceptible to long-term failure and inflammatory reactions.

Moreover, PGs can be used as controlled local delivery systems for therapeutic molecules (*e.g.* antimicrobial ions and growth factors) that are slowly released as the implant degrades. *In-situ* controlled delivery avoids the need for oral administration and injection, improving the quality of life of patients. As the ions released from PGs already exist in the body, low toxicity and good biocompatibility is guaranteed.[12]

Mesoporous materials are usually prepared in solution via supramolecular chemistry using surfactants, which templates the inorganic material. Surfactants spontaneously organise (self-assemble) in specific-shaped micelles at the critical micellar concentration, the shape and size depending on the specific surfactant used.[3] After removal of the surfactant via calcination or solvent exchange, pores having the sizes of the micelles are left in the inorganic material. The conventional melt-quench method (MQ) of preparing PGs cannot be used for the synthesis of MPGs because it requires melting of oxide powders at temperatures >1100 °C and rapid cooling.[13] Moreover, this method often leads to non-homogeneous, bulk glasses that cannot be used for hosting temperature sensitive molecules.[14]

The sol-gel process (SG), a wet chemical bottom-up technique based on the hydrolysis and polycondensation of precursors in solution, has been found to be an excellent alternative synthetic route to MQ for the production of PGs.[8, 15, 16] In particular, the SG process is ideal for the synthesis of mesoporous systems. Surfactant molecules can be easily added using the SG method into the precursor solutions and the morphology of pores can be tailored thanks to the easily controlled solution-based chemistry. Silicate-based glasses in the SiO_2-CaO-Na_2O-P_2O_5 system synthesised via the SG method have shown to bond to living bone through the formation of a hydroxyl carbonate apatite (HCA) layer on their surface.[17] It has been shown

that the much higher porosity and surface area, as a result of the mesoporous structure, enhances the bioactivity of silicate-based sol-gel glasses by accelerating the rate of HCA formation and providing an ideal support for cell growth and supply of nutrients.[18, 19] Given that the composition of PGs is much more similar to the composition of bone and teeth than in the case of silicate-based glasses,[20] MPGs are expected to induce HCA formation on their surface. As observed in silicate-based glasses, introduction of mesoporosity into the PGs is expected to accelerate the kinetic deposition process of HCA that favours bone formation.[3]

Mesoporous silicate-based glasses have also been used to host, protect and deliver drug molecules to the target sites.[21] Recent studies have shown high dosages of antimicrobial drug molecules can be loaded into mesoporous silicate-based glasses to deliver appropriate drug concentrations to sites of infection with minimum side effects.[21, 22] Introduction of mesoporosity into PGs would enhance the potential applications of these materials as controlled drug delivery systems, as the majority of drugs used in clinical practise can easily be hosted in the mesopores.[5] Moreover, similar to the mesoporous silicate-based glasses, the surface of MPGs can be functionalised to avoid burst release and facilitate delivery of drug molecules to the specific site of action.[23, 24]

In the present work, we have synthesised for the first time, a mesoporous calcium phosphate-based glass. Bioactivity and biocompatibility were investigated by monitoring HCA formation and by seeding Saos-2 cells on the glass surface, respectively. Drug loading efficiency and controlled release were investigated by incorporating into the glass tetracycline hydrochloride (TCH), a commonly used antibiotic that inhibits protein synthesis.[25] Results show that the presence of a mesoporous structure clearly enhances bioactivity, biocompatibility, and drug loading capability of the phosphate-based glasses. Therefore, MPGs have potential to be used as multifunctional bioresorbable systems, in particular for bone regeneration, by combining formation of new bone tissue with controlled delivery of therapeutic molecules.

2. MATERIALS AND METHODS

2.1. Materials

The following chemicals were used without further purification: n-butyl phosphate (1:1 molar ratio of mono $OP(OH)_2(OBu)$ and di-butyl phosphate $OP(OH)(OBu)_2$, Alfa Aesar, 98%), calcium methoxyethoxide (Ca-methoxyethoxide, abcr, 20% in methoxyethanol), sodium methoxide solution (NaOMe, Aldrich, 30 wt% in methanol), ethanol (EtOH, Fisher, 99%), and Pluronic (P123, M_n=5800, Aldrich).

2.2. Synthesis method

1.7 g of n-butyl phosphate were added to 5 mL of EtOH in a dried vessel and left under stirring for 10 minutes. 3.5 g of Ca-methoxyethoxide and 0.5 g of NaOMe were then added dropwise into the mixture while stirring; the solution was kept under stirring for about 1 h. The mixture was then divided into two parts: one was used to obtain mesoporous phosphate-based glasses (MPGs) and the other was used to prepare non-porous phosphate-based glasses (PGs) for comparison purposes. In order to prepare MPG, 2.5 g of P123 were dissolved in 5 mL of EtOH and 2.5 mL of water, added to the initial mixture and allowed to react for 10 minutes. For the preparation of PGs, the initial mixture was used with no addition of P123. PG and MPG mixtures were then poured into glass containers and allowed to gel at room temperature. Both mixtures turned to gel after about 10 minutes and they were aged for 1 day at room temperature. Gels were then dried using a multi-step drying ramp: the temperature was increased from room temperature to 40 ˚C and held for 1 day, then to 60 °C and held for 2 days, then to 80 °C and held for 2 days and finally to 120 °C and held for 1 day. A calcination step was then performed by heating the glasses to 300 °C and holding at this temperature for 1 h to remove the surfactant and any remaining solvents from the sample. A heating rate of 1 $°C \cdot min^{-1}$ was used in all steps in order to prevent the collapse of the mesoporous structure. The obtained glasses were ground

at 10 Hz to form microparticles (MM301 milling machine, Retsch GmbH, Hope, UK) and microparticles in the size range of 106–200 μm were obtained using test sieves (Endecotts Ltd, London, UK). A schematic illustration of the synthesis of MPG is presented in **Figure 1**.

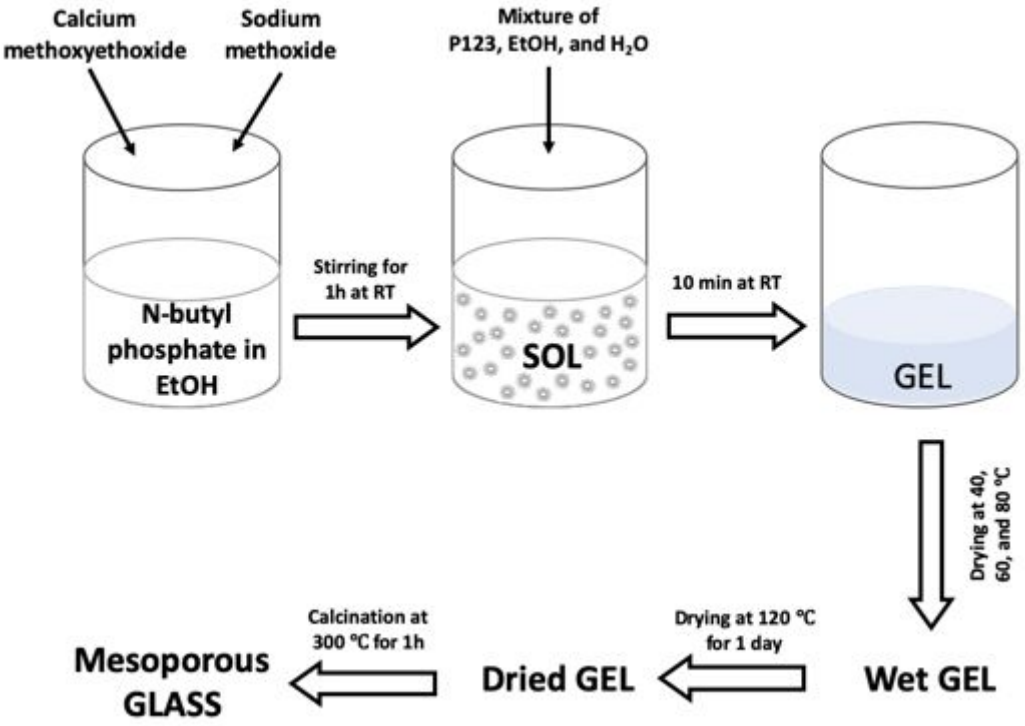

Figure 1. Flow diagram for the preparation of MPG.

2.3. Characterisation

Wide angle X-ray diffraction (WA-XRD, PANalytical X'Pert, Royston, UK) was performed in flat plate geometry using Ni filtered Cu Kα radiation. Scans were collected using a PIXcel-1D detector with a step size of 0.0525° over the 2θ range 10-90° with a count time of 12 s per step. Low angle X-ray diffraction (LA-XRD, PANalytical X'Pert, Royston, UK) was performed using Ni filtered Cu Kα radiation in transmission mode using a focusing mirror on

the X-ray incident beam. Scans were collected using a PIXcel-3D detector with a step size of 0.0525° over the 2θ range 0.3–6.0° with a count time of 0.017 s per step.

Scanning electron microscopy (JSM-7100F, Jeol, Welwyn, UK) was performed at an accelerating voltage of 5 kV and working distance of 10.0 mm. The samples were mounted onto an aluminium stub using carbon conductive tape. The Image-pro plus software (Media Cybernetics, USA) was used for image analysis. Energy Dispersive X-ray spectroscopy (EDX) was performed using a scanning electron microscope (MagnaRay, ThermoFisher, Hemel Hempstead, UK) operating at 20 kV, with spot size 6 and a working distance of 10 mm.

Solid state ^{31}P MAS NMR spectra (^{31}P MAS-NMR, AVANCE III, Bruker, Coventry, UK) were recorded at 161.87 MHz using direct excitation with a 90° pulse and 60 s recycle delay at ambient probe temperature (~ 25 ℃). Between 20 and 88 scans were acquired in each case. Powder samples were loaded into a 4.0 mm diameter (outside diameter) zirconia rotor and spun at 12 kHz. Spectra were referenced to the resonance of the secondary reference ammonium dihydrogen phosphate ($NH_4H_2PO_4$) at 0.9 ppm (relative to 85% H_3PO_4 solution at 0 ppm). Spectra were fitted using the Dmfit software package.[26]

Fourier Transform Infrared (FT-IR, 2000 series, Perkin Elmer, Seer Green, UK) spectra were acquired in attenuated total reflectance mode (Golden Gate, Specac, Orpington, UK) using the Timebase software (Perkin Elmer). Spectra were collected at room temperature in absorbance mode in the wavenumber range of 600-1500 cm^{-1}.

Surface area, pore size and pore volume were obtained from N_2 adsorption-desorption measurements (Gemini V, Micromeritics, Hertfordshire, UK) at 77 K; in particular, the specific surface area (SSA) was assessed by using the Brunauer-Emmet-Teller (BET) method, whereas the pore size distribution was determined from the desorption branch of the isotherm through the Barrett-Joyner-Halenda (BJH) method. Samples were outgassed at 270 °C for 6 h prior to the measurements.

TCH release was assessed via UV-Vis spectroscopy using a Libra, BioChrom, Cambridge, UK in the range 320-450 nm.

2.4. Dissolution studies and pH changes

Dissolution studies were performed by soaking 10 mg of the MPG and PG powders in 10 mL of deionised water for up to 7 days. The experiment was carried out in triplicates (n = 3). The resulting suspensions for each time point were centrifuged at 4800 rpm for 10 min to separate the undissolved samples from the solution. Concentration of phosphorus, calcium, and sodium in the solution were measured by inductively coupled plasma-optical emission spectroscopy (ICP-OES, 720ES-Varian, Crawley, UK) calibrated across the predicted concentration range using a multi-element standard solution (VWR, Lutterworth, UK). Both samples and standards were diluted in 1:1 in 4% HNO_3 (Fluka) and analysed with reference to a blank solution (2% HNO_3) under standard operating conditions (Power: 1350 W; Coolant Flow: 15.0 $L \cdot min^{-1}$: Axillary Flow: 1.0 $L \cdot min^{-1}$).

Changes of pH over time were investigated by soaking 10 mg of the MPG and PG powders in 10 mL of deionised water (pH = 7.0 ± 0.1) and cell culture medium (pH = 7.8 ± 0.1). The solutions were stored at 37 °C and the pH was measured for up to 7 days with three replicates for each time point using an Orion pH meter (Thermo scientific-Orion star, Loughborough, UK).

2.5. *In vitro* bioactivity and biocompatibility assessment

In vitro bioactivity was evaluated by immersing 25 mg of MPG and PG powders in 25 mL of simulated body fluid (SBF), a solution with ion concentrations very similar to human blood plasma,[27] stored in an incubator at 37 °C while shaking at 100 rpm for 24 h. The samples were

then washed with water and ethanol and finally dried at 60 °C for 6 h before WA-XRD characterisation and observation of their surfaces with SEM.

In vitro biocompatibility was assessed by seeding Saos-2 cells (HTB85, ATCC, UK) on MPG and PG powders. Saos-2 cells were chosen as representative of osteoblast behaviour and cultured in medium (McCoy's 5a, ATCC, UK) with 15% fetal bovine serum (FBS, Gibco, Invitrogen, Loughborough, UK) and 1% Antibiotic-Antimycotic (Thermo Scientific, Loughborough, UK) in a humidified incubator at 37 °C and 5% CO_2. On reaching 90% confluency, cells were passaged and used for cytocompatibility analysis. To facilitate the attachment of the cells on to the MPG and PG powders for SEM imaging, polycarbonate cell culture inserts with 0.4 μm pore size (Millipore, Merck, UK) were used. 10 mg of MPG and PG powders were placed on the inserts and incubated with the medium overnight. Approximately 1.2×10^4 cells were placed in each insert and cultured for 7 days with cell viability assessment during the culture period. Cells only on inserts were used as a control for comparison purposes.

SEM was used to visualise cell attachment and growth on MPG and PG surfaces. At the end of day 7, cells were fixed with 3% glutaraldehyde (Sigma-Aldrich) followed by dehydration using graded ethanol. Samples were then air dried, gold sputter coated and visualised using SEM. To visualise the nucleus and actin filaments, cells were fixed using 4% paraformaldehyde and stained with DAPI- Phalloidin at the end of day 7. Samples were incubated for 20 min at room temperature in staining solution containing 2.5 μL of DAPI (1 $mg \cdot mL^{-1}$ stock solution), 4 μL of Phalloidin (200 $U \cdot mL^{-1}$ stock concentration, Alexa Fluor 488, Phalloidin, Life Technologies) and 20 μL of Triton X per mL of PBS. Cells were then visualised using a cell image multi-mode reader (Cytation-5, BioTek, Swindon, UK).

2.6. Drug loading and *in vitro* drug release study

To assess the intake of drugs for controlled delivery applications of MPG and PG, tetracycline hydrochloride (TCH) was added to the samples via impregnation. 5 mg of MPG and PG powders were soaked in 5 mL TCH solution prepared by adding 5 mg TCH in 5 mL of ethanol. The mixtures were stirred for 60 min at room temperature and then centrifuged at 4800 rpm for 5 min to separate the impregnated glass particles from the solutions. The glasses impregnated with TCH were then washed once with ethanol and centrifuged to remove the excess of unloaded TCH. The glasses were then dried overnight at room temperature. TCH release was assessed by adding 5 mL of deionised water to the samples, keeping them in an incubator at 37 °C under shaking at 100 rpm and collecting the solution at different time points up to 24 h. Three replicates for each time point were measured.

TCH release was assessed via UV-Vis spectroscopy using a Libra, BioChrom, Cambridge, UK in the range 320-450 nm.

3. RESULTS AND DISCUSSION

Chemical analysis of MPG and PG samples was carried out using SEM equipped with an EDX detector in order to determine their exact compositions. **Table 1** reports compositions expressed in terms of oxide mol %; elemental compositions in terms of weight % and mol % along with the EDX spectra are reported in **Table S1** and **Figure S1**, respectively. As expected, MPG and PG samples have very similar compositions (P_2O_5 ~ 45-46 mol %, CaO ~ 35-36 mol % and Na_2O ~ 19 mol %). The oxide content was chosen on the basis of previous studies on MQ and SG phosphate-based glasses. Glasses with P_2O_5 content in the range 40-50 mol % and CaO content in the range 20-40 mol % have been shown to have good bioactivity and biocompatibility.[15, 28]

Table 1. Compositions of MPG and PG measured by EDX.

Glass Code	Oxides (mol %)		
	P_2O_5	CaO	Na_2O
MPG	45.0 (±1.2)	36.0 (±0.9)	19.0 (±0.5)
PG	46.0 (±0.9)	35.0 (±0.7)	19.0 (±0.6)

In order to assess the amorphous nature of synthesised samples, WA-XRD was performed. The WA-XRD patterns, reported in **Figure 2A**, do not show any Bragg peaks, with only broad halo centred at around 2θ ~ 28°, clearly indicating that both samples are fully amorphous. Despite similar content and WA-XRD patterns, MPG and PG are expected to show very different textural properties given that only MPG was synthesised using the templating agent P123. This was confirmed by N_2 adsorption and desorption analysis at 77 K (**Figure 2B**). MPG shows an adsorption-desorption isotherm that can be classified as type IV, characteristic of mesoporous solids, whereas PG, which does not show an adsorption-desorption isotherm, is clearly non-porous. The shape of the MPG hysteresis loop can be classified as type H1, which is typical of cylindrical pores arranged in a hexagonal manner open at both ends.[29] The presence of cylindrical pores is in agreement with the type of surfactant used (P123) which is known to form cylindrical micelles, which aggregate forming two dimensional hexagonal arrangements,[3] leaving hexagonal arrays of unidirectional cylindrical pores after calcination. MPG presents a narrow, single modal pore size distribution centred at around 12 nm (inset of **Figure 2B**). The surface area calculated using the BET model is 124 $m^2 \cdot g^{-1}$ and the pore volume is 0.28 $cm^3 \cdot g^{-1}$. Despite the surface area being lower than typical mesoporous silicate-based glasses, the result is remarkable as it is the first example ever reported of a mesoporous calcium phosphate-based glass, which are known to have a much weaker network structure than silicate-based ones.[8] The size of the mesopores is also ideal as 12 nm pores can easily accommodate the majority of

drug molecules of interest in clinical applications.[7] Further evidence of the presence of mesopores in MPG was given by SEM analysis. The SEM image reported in **Figure 2C** clearly shows a highly porous structure with a pore size range of 10-20 nm, in good agreement with the pore size distribution obtained via N_2 adsorption at 77 K. A wall thickness of 4-5 nm was estimated from SEM images which is in agreement with typical values found in mesoporous silicate-based glasses prepared using P123 as a surfactant.[30] Moreover, by looking carefully at the local arrangement of pores, a hexagonal arrangement of mesopores can be seen (zoomed area in **Figure 2C**), suggesting a certain local order of mesopores. This is in agreement with the type H1 hysteresis loop observed in the N_2 adsorption-desorption isotherm. The SEM images of PG, reported in **Figure S2**, do not show any porosity, as expected.

In order to further investigate the arrangement of mesopores in MPG, LA-XRD was performed on MPG and also on PG for comparison (**Figure 2D**). MPG shows a strong reflection at $2\theta = 0.8°$ and a broader reflection at $2\theta = 2.6°$, consistent with a degree of order in the arrangement of pores. These reflections can be assigned to the (100) and (200) sets of planes, respectively, in the 2D hexagonal mesoporous porous structure.[9, 31] As expected for a non-porous system, no reflections were observed in the PG sample.

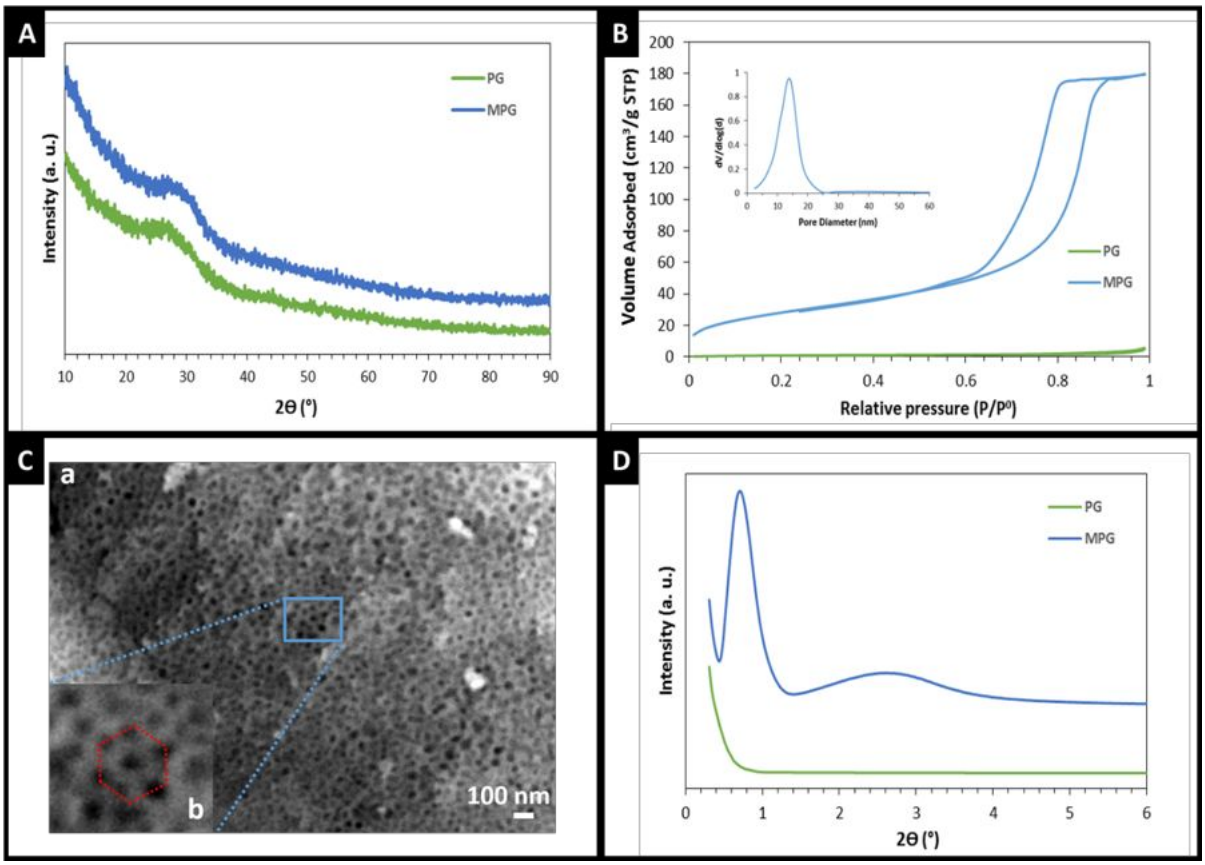

Figure 2. Characterisation of MPG and PG samples: **(A)** WA-XRD patterns, **(B)** N_2 adsorption and desorption isotherms; inset: BJH pore size distribution, **(C)** SEM image of MPG **(a)**; detail of blue squared area **(b)**, and **(D)** LA-XRD patterns.

The textural properties of MPG and PG are clearly very different as expected. It is therefore interesting to investigate if the different morphologies affect the structural properties, in particular the way the phosphate chains are linked. ^{31}P MAS NMR is a very powerful tool for the investigation of the local environment around phosphorus and the connectivity of the phosphate units. The ^{31}P MAS NMR spectra of both MPG and PG samples are presented in **Figure 3A**. Resonances are assigned to Q^n phosphate species, where *n* represents the number of bridging oxygens between phosphate units. Both spectra show a main resonance at about -6 ppm ascribed to Q^1 groups with a relative intensity in the range 68-73% and a less intense

resonance (27-32%) at about -23 ppm ascribed to Q^2 groups (**Table S2**). Results are in agreement with previous studies on non-porous SG phosphate-based glasses of similar composition that show a structure dominated by Q^1 groups with a smaller percentage of Q^2.[12]

A confirmation of the fact that the textural properties do not affect the structure of the phosphate chains is given by FT-IR spectroscopy. As shown in **Figure 3B**, the FT-IR spectra of MPG and PG, measured in the range 600-1500 cm^{-1} are very similar. The band at ~1100 cm^{-1} and the shoulder at ~1235 cm^{-1} can be assigned to the asymmetric stretching υ_{as} $(PO_3)^{-2}$ and υ_{as} (PO_2) modes, respectively, related to Q^1 and Q^2 phosphate units, respectively. The band at ~900 cm^{-1} and the less intense band at ~730 cm^{-1} can be assigned to the asymmetrical stretching mode υ_{as} (P-O-P) and symmetrical stretching mode υ_s (P-O-P), respectively (Q^2 phosphate units).[32, 33]

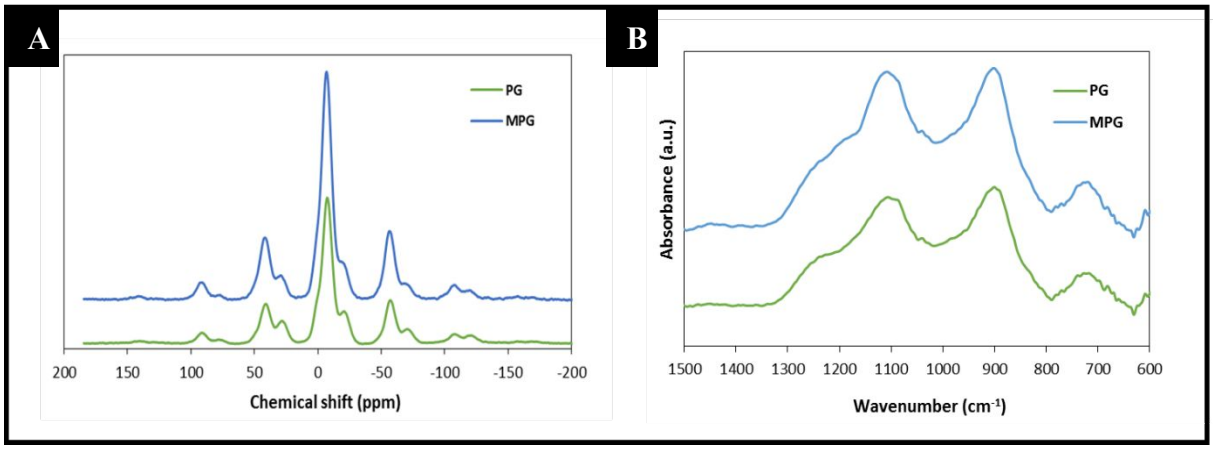

Figure 3. (A) ^{31}P MAS NMR and **(B)** FT-IR spectra of MPG and PG samples.

As phosphate-based glasses have great potential as bioresorbable materials, it is important to assess their potential as controlled delivery systems. In particular, it is interesting to compare the dissolution properties of MPG and PG, given that the two systems have very

different textural properties, but similar structure. The release of phosphorus, calcium, and sodium in deionised water at different time points up to 7 days was measured via ICP-OES and data presented in **Figure 4A**, **4B** and **4C**, respectively. Results show that release profiles do not change significantly with change in porosity, especially during the first 8 h. In particular, P release is identical in MPG and PG samples for the first 8 h, Ca release is identical for the first 12 h and Na release is identical for the first 72 h. Dissolution trends that follow the initial overlapping release are similar for MPG and PG systems. However, a slightly higher amount of P, Ca and Na is released over time by the MPGs system.

Along with the dissolution products, pH change was also monitored over time. pH monitoring is important in order to evaluate the potential application of MPGs as biomaterials. pH change was monitored in both deionised water and cell culture medium over a period of 7 days (**Figure 4D**). pH changes of MPG and PG samples over time follow a similar trend, as observed for the release of P, Ca and Na. However, the pH values for PG are slightly higher than for MPG. The pH values measured in deionised water remain relatively neutral, dropping from 7.0 to ~6.2 after 8 h, increasing slightly up to 24 h and then remaining stable up to 7 days at around 6.4. The pH values measured in cell culture medium drop from 7.8 to 7.4 after 8 h, increasing slightly up to 24 h and then remaining stable up to 7 days around 7.6. The initial pH reduction can be ascribed to the dissociation of phosphate anions released with formation of phosphoric acid.[34] The slight increase in pH following that can be related to the presence of Na^+ ions in the solution.

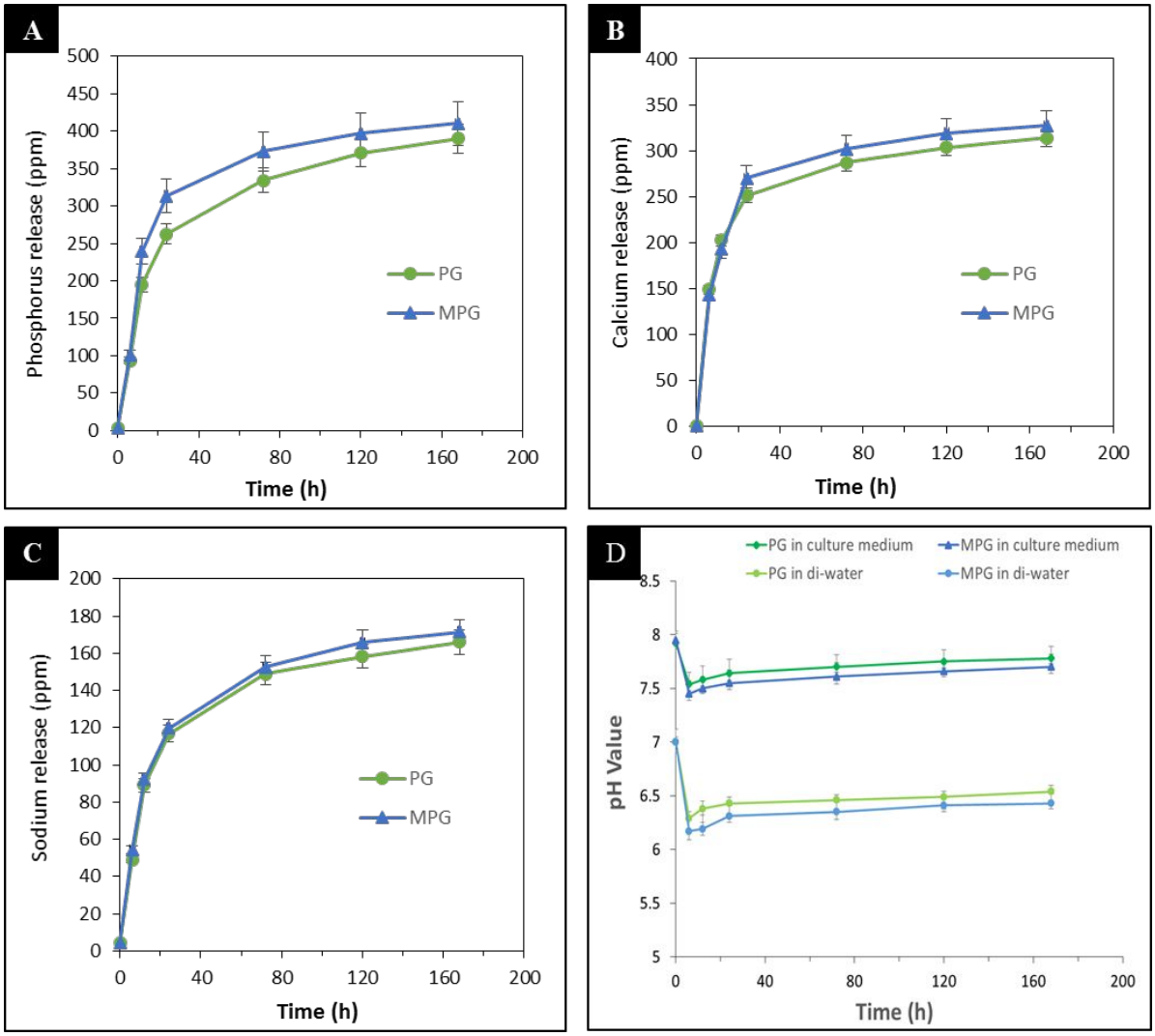

Figure 4. Release of **(A)** phosphorus, **(B)** calcium, and **(C)** sodium in deionised water measured by ICP-OES and **(D)** pH change in deionised water and cell culture medium as a function of time for MPG and PG samples.

Dissolution studies have shown that P, Ca and Na can be released in a controlled way. The capability of releasing phosphate and calcium ions has been linked to the bioactivity of glasses, in particular with the formation of HCA on the glass surface when in contact with the damaged bone site.[35] As HCA is a naturally occurring mineral present in bones and teeth, the formation of HCA can be used as indication of the bioactivity (osseointegration) of MPGs.[36]

Previous studies have shown that mesoporous silicate-based glasses have superior *in vitro* bioactivity and *in vivo* osteogenic properties compared to the corresponding non-porous systems.[37] However, to the knowledge of the authors, no work has been done on bioactivity of phosphate-based glasses synthesised via sol-gel route. It is therefore interesting to investigate the capability of MPG and PG in forming HCA on their surface. The *in vitro* bioactivity of the MPG and PG samples was investigated by immersing the glasses in SBF for 24 h. As shown in **Figure 5A**, the WA-XRD pattern of MPG after immersion in SBF clearly indicates the precipitation of a crystalline phase that can be ascribed to HCA (ICDD card No. 24-0033). On the other hand, no crystallisation is observed on the surface of PG. XRD results are confirmed by FT-IR analysis, performed before and after immersion of MPG in SBF (**Figure S3**). After immersion, two bands at 1037 cm^{-1} and 962 cm^{-1} can be observed, corresponding to the antisymmetric and symmetric P-O stretching mode, respectively. These band have been ascribed to nanocrystalline HA.[38]

Results are confirmed by SEM analysis that clearly shows formation of HCA nanocrystals on the surface of MPG, but not PG (**Figure 5B** and **5C**).

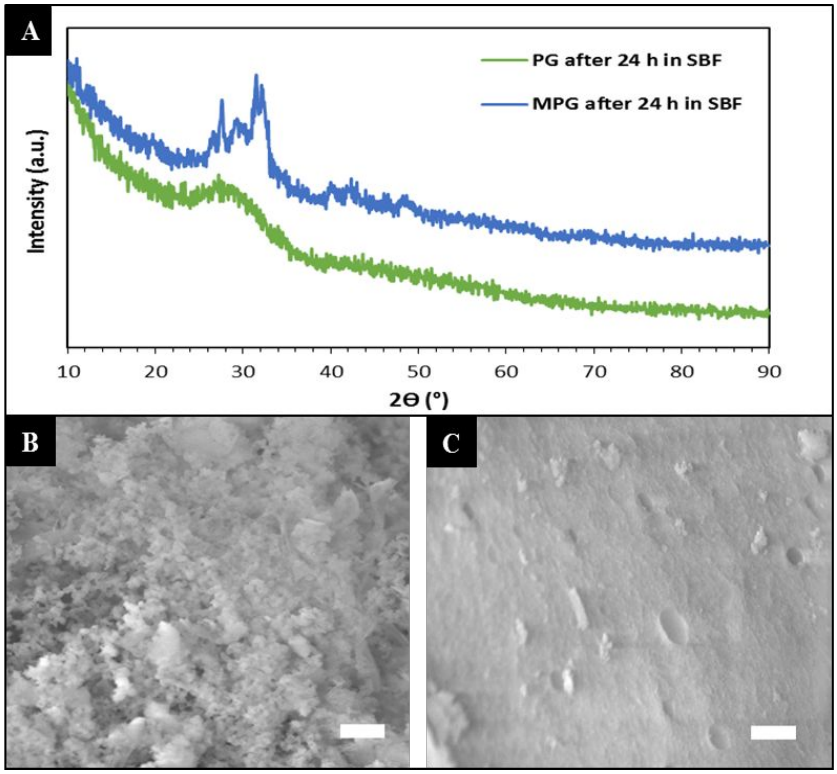

Figure 5. (A) XRD patterns of MPG and PG; SEM images of **(B)** MPG and **(C)** PG after immersion in SBF for 24 h at 37 °C. The scale bar is 1 μm.

It is not excluded that HCA could also form inside the mesopores given that the surface area of MPG after immersion in SBF is lower than before immersion (63 $m^2 \cdot g$). Also, the absorption-desorption hysteresis loop of has changed, as reported in **Figure S4**.

It is interesting to note that despite the release of P, Ca and Na being quite similar in MPG and PG (as shown in the dissolution studies), *in vitro* bioactivity is greater in MPG (as demonstrated by HCA formation on MPG only). Moreover, the composition of MPG and PG is identical. Therefore, these results indicate that higher bioactivity can be achieved solely by changing the textural properties of the system. In particular, results clearly show that the mesoporosity increases the rate of HCA formation on the surface of MPG and likely also inside the mesopores". This suggests that high surface area and high porosity allow a better diffusion of physiological fluids into the glass, which could be responsible for the enhancement of the kinetic of processes at the interfaces.[3] Difference in bioactivity cannot be ascribed to a change

in the local structure, given that ^{31}P MAS NMR has shown the presence of the same phosphate units (Q^1 and Q^2) in similar amounts and FT-IR spectra are also very similar.

Given the very promising results on osseointegration of MPG, biocompatibility was assessed by evaluating viability and attachment of Saos-2 osteosarcoma cells cultured on its surfaces. These cells were selected because they possess several osteoblastic features and can therefore be used to mimic the osteoblast response to the glasses.[39] Saos-2 cells were also cultured on PG for comparison purposes. The control consisted of Saos-2 cells seeded directly on a cell culture support.

Cell viability was quantitatively assessed using the Alamar Blue fluorescence assay after 1, 3, 5, and 7 days. The graph shown in **Figure 6A** represents the change in fluorescence of Alamar Blue dye as a direct indicator of cellular metabolic activity which is directly linked to the number of cells. Cell growth does not change significantly in the first 3 days for PG; however, MPG shows a slight increase after day 3. At day 5 and 7, both MPG and PG show an increase cell proliferation. However, MPG clearly shows higher cell proliferation than PG.

Cell attachment was assessed via SEM and DAPI-Phalloidin staining. **Figure 6B** shows SEM images of Saos-2 cells well attached and widely spread on the surface of MPG and PG over a 7-day period. SEM results were confirmed by qualitative analysis based on DAPI-Phalloidin staining (**Figure 6C**). Cell nuclei (blue) and filaments (green) show that cells are attached and spread on MPG and PG surfaces after 7 days of seeding.

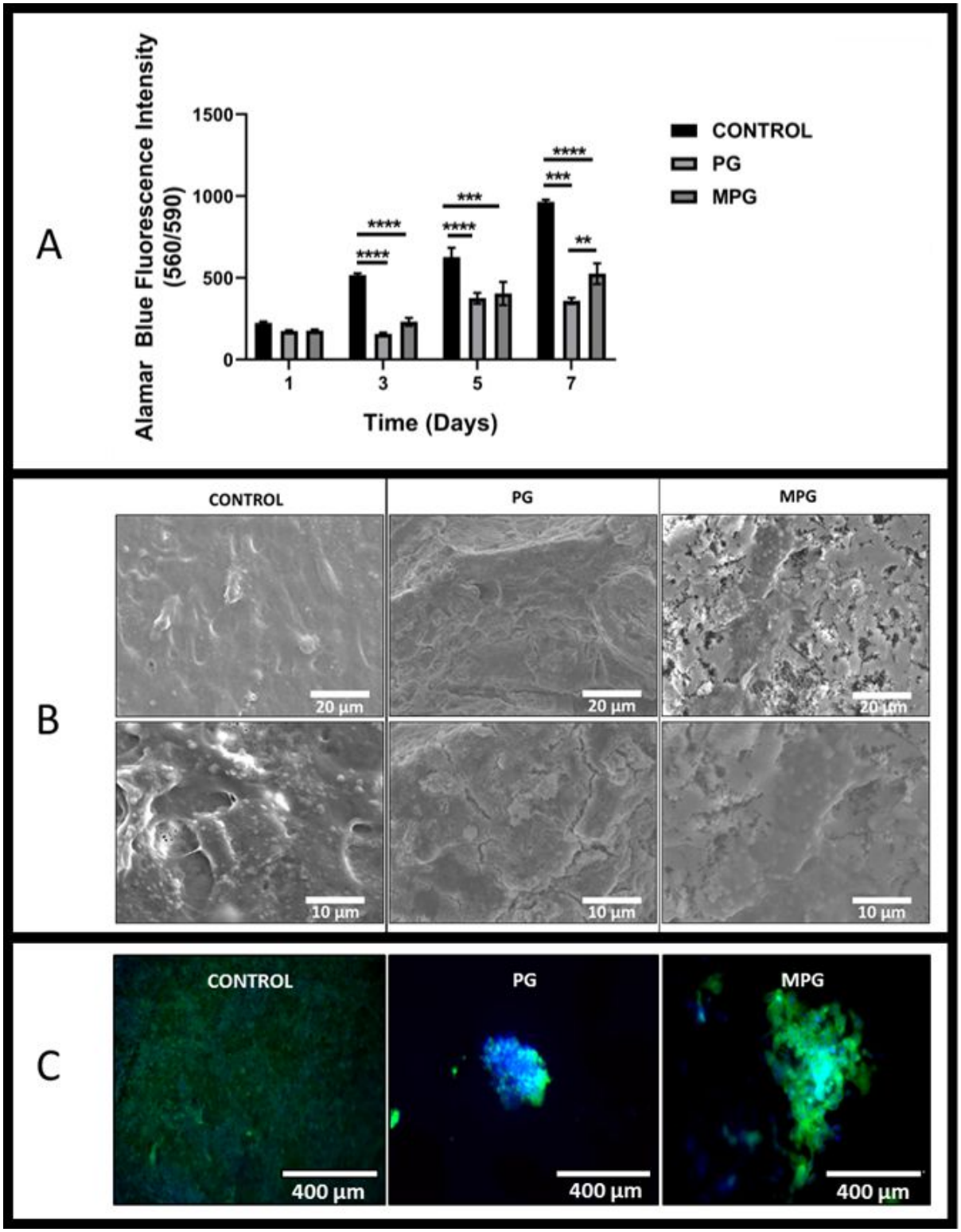

Figure 6. (A) Saos-2 cell viability measurement using the Alamar Blue fluorescence assay after 1, 3, 5 and 7 days; error bars are SD (n = 3); **(B)** SEM images showing Saos-2 cells attachment after 7 days at two different magnifications; **(C)** DAPI- Phalloidin staining after 7 days for the MPG and PG samples.

Mesoporous silicate-based glasses have been shown to be excellent drug loading and release systems thank to the extended porosity.[5, 21] Therefore, MPGs are also expected to show enhanced drug intake and controlled release. This was investigated using tetracycline hydrochloride (TCH) as a model antibiotic, often administrated to patients after surgery to avoid bacterial infections. MPG and PG samples were loaded with TCH by impregnation. The release of TCH in deionised water was then studied over a period of 24 h (**Figure 7**). The loaded MPG shows a sharp TCH release in the first hour (100 μg) followed by a sustained release reaching to 130 μg after 24 h. However, loaded PG shows a total release of about 30 μg within the first 30 min. Given that the dissolution properties of the MPG and PG samples in deionised water are very similar, the different TCH release behaviour can be ascribed to a different TCH loading and texture. In particular, the high porosity and surface area of the MPG system allows for a significantly higher drug loading than the non-porous PG, which explains the higher release of TCH from loaded MPG in comparison to loaded PG.

The higher loading of TCH in MPG compared to PG was confirmed by measuring the UV-Vis spectra of TCH remaining in the supernatant solution after impregnation. Figure S5 shows that the amount of TCH remaining in the supernatant solution is higher after impregnation of PG than MPG, indicating a lower amount of TCH absorbed in PG. This is in agreement with previous results reported in literature on mesoporous silicate-based glasses which have been shown to have much higher loading efficiency than the non-porous ones.[40]

Moreover, loaded MPG shows a more sustained release during the 24 h of the study. This could be explained considering that TCH molecules are initially incorporated into the mesopores and then slowly released.[41] It is interesting to note that differently from TCH release, ion release does not change significantly with porosity. This can be explained by the fact that ions are added into the phosphate network before formation of the mesoporous

structure whereas TCH has been added to the glass via impregnation of the mesoporous structure.

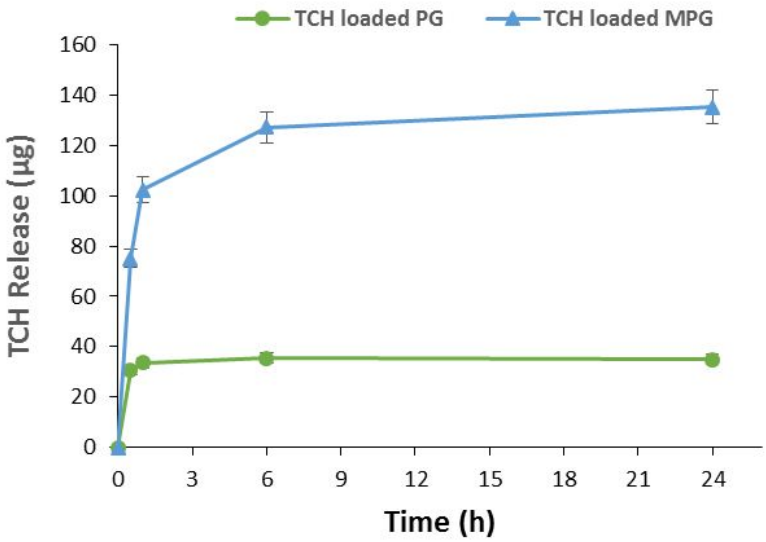

Figure 7. Release profiles of TCH as a function of time from loaded MPG and PG samples.

4. CONCLUSIONS

This study presents the first example of a mesoporous calcium phosphate-based glass ever reported and investigates its potential applications as multifunctional material for controlled drug delivery and bone tissue regeneration. MPG, prepared using a combination of sol-gel chemistry and supramolecular templating, has a surface area of 124 $m^2 \cdot g^{-1}$, an average pore size of 12 nm, and pore volume of 0.28 $cm^3 \cdot g^{-1}$. ^{31}P MAS-NMR results show that it is mainly formed by Q^1 groups (68%) and Q^2 groups (32%). Dissolution studies have shown gradual release of P, Ca and Na over time which makes it excellent candidate as controlled delivery system. Moreover, pH remains near neutral upon dissolution in cell medium. A comparison between MPG and non-porous glass of the same composition (PG) shows that they have similar structure and dissolution properties. However, they show very different *in vitro* bioactivity,

biocompatibility and drug loading/release properties because of their different textural properties. Presence of mesoporosity has shown enhancement of the kinetics of HCA formation, which appears on the surface of MPG within the first 24 h of immersion in SBF. Cytotoxicity studies indicate that mesoporosity also enhances Saos-2 osteosarcoma cells attachment and proliferation on the surfaces of the glasses. Studies on incorporation and release of the antibiotic TCH into MPG have shown that the extended porosity and high surface area allow for a higher loading and more controlled release over time compared to the analogous non-porous system PG. The novel synthetic route presented in this work opens new horizons in designing a new generation of non- siliceous, mesoporous glasses with great potential in tissue engineering and drug delivery systems.

SUPPORTING INFORMATION AVAILABLE

The following files are available free of charge: details of elemental compositions measured by Energy dispersive X-ray spectroscopy (EDX); EDX spectra; ^{31}P MAS NMR spectral parameters.

ACKNOWLEDGMENTS

The authors would like to acknowledge EPSRC (grant EP/P033636/1) and Royal Society (grant RSG\R1\180191) for providing the funding to conduct this study. The authors are also grateful to Dr David Jones for his help with the SEM/EDX and Dr Graham Palmer for his help with ICP-OES measurements.

Conflict of interest

The authors declare no conflict of interest.

REFERENCES

(1) Moritz Michal; Malgorzata Geske-Moritz. Mesoporous Materials as Multifunctional Tools in Biosciences: Principles and Applications. *Mater. Sci. Eng. C* **2015**, *49*, 114–151. https://doi.org/10.1016/j.msec.2014.12.079.

(2) Wu, C.; Chang, J. Mesoporous Bioactive Glasses: Structure Characteristics, Drug/Growth Factor Delivery and Bone Regeneration Application. *Interface Focus* **2012**, *2*, 292–306. https://doi.org/10.1098/rsfs.2011.0121.

(3) Izquierdo-barba, I.; Access, O. Mesoporous Bioactive Glasses : Relevance of Their Porous Structure Compared to That of Classical Bioglasses. *Biomed. Glas.* **2015**, *1*, 140–150. https://doi.org/10.1515/bglass-2015-0014.

(4) Yang, P.; Gai, S.; Lin, J. Functionalized Mesoporous Silica Materials for Controlled Drug Delivery. *Chem Soc Rev* **2012**, *41*, 3679–3698.

(5) Vallet-Regí, M.; Balas, F.; Arcos, D. Mesoporous Materials for Drug Delivery. *Angew. Chemie - Int. Ed.* **2007**, *46*, 7548–7558. https://doi.org/10.1002/anie.200604488.

(6) Zhang, X.; Zeng, D.; Li, N.; Wen, J.; Jiang, X.; Liu, C.; Li, Y. Functionalized Mesoporous Bioactive Glass Scaffolds for Enhanced Bone Tissue Regeneration. *Sci. Rep.* **2016**, *6* (October 2015), 19361. https://doi.org/10.1038/srep19361.

(7) Vallet-Regí, M. Ordered Mesoporous Materials in the Context of Drug Delivery Systems and Bone Tissue Engineering. *Chem. - A Eur. J.* **2006**, *12*, 5934–5943. https://doi.org/10.1002/chem.200600226.

(8) Owens, G. J.; Singh, R. K.; Foroutan, F.; Alqaysi, M.; Han, C. M.; Mahapatra, C.;

Kim, H. W.; Knowles, J. C. Sol-Gel Based Materials for Biomedical Applications. *Prog. Mater. Sci.* **2016**. https://doi.org/10.1016/j.pmatsci.2015.12.001.

(9) Tian, B.; Liu, X.; Tu, B.; Yu, C.; Fan, J.; Wang, L.; Xie, S.; Stucky, G. D.; Zhao, D. Self-Adjusted Synthesis of Ordered Stable Mesoporous Minerals by Acid-Base Pairs. *Nat. Mater.* **2003**, *2* (3), 159–163. https://doi.org/10.1038/nmat838.

(10) Kyffin, B. A.; Foroutan, F.; Raja, F. N. S.; Martin, R. A.; Pickup, D. M.; Taylor, S. E.; Carta, D. Antibacterial Silver-Doped Phosphate-Based Glasses Prepared by Coacervation. *J. Mater. Chem. B* **2019**. https://doi.org/10.1039/C9TB02195G.

(11) Lapa, A.; Cresswell, M.; Jackson, P.; Boccaccini, A. R.; Lapa, A.; Cresswell, M.; Jackson, P.; Boccaccini, A. R.; Lapa, A.; Cresswell, M. Phosphate Glass Fibres with Therapeutic Ions Release Capability – a Review. *Adv. Appl. Ceram.* **2019**, 1–14.

(12) Foroutan, F.; Jokerst, J. V.; Gambhir, S. S.; Vermesh, O.; Kim, H. W.; Knowles, J. C. Sol-Gel Synthesis and Electrospraying of Biodegradable $(P_2O_5)_{55}$-$(CaO)_{30}$-$(Na_2O)_{15}$ glass Nanospheres as a Transient Contrast Agent for Ultrasound Stem Cell Imaging. *ACS Nano* **2015**. https://doi.org/10.1021/nn506789y.

(13) Ahmed, I.; Lewis, M.; Olsen, I.; Knowles, J. C. Phosphate Glasses for Tissue Engineering: Part 1. Processing and Characterisation of a Ternary-Based P_2O_5–CaO–Na_2O Glass System. *Biomaterials* **2004**, *25* (3), 491–499.

(14) Kaur, G.; Pickrell, G.; Sriranganathan, N.; Kumar, V.; Homa, D. Review and the State of the Art: Sol–Gel and Melt Quenched Bioactive Glasses for Tissue Engineering. *Journal of Biomedical Materials Research - Part B Applied Biomaterials*. 2016. https://doi.org/10.1002/jbm.b.33443.

(15) Carta, D.; Pickup, D. M.; Knowles, J. C.; Smith, M. E.; Newport, R. J. Sol-Gel Synthesis of the P(2)O(5)-CaO-Na(2)O-SiO(2) System as a Novel Bioresorbable Glass. *J. Mater. Chem.* **2005**, *15* (21), 2134–2140. https://doi.org/10.1039/b414885a.

(16) Carta, D.; Knowles, J. C.; Smith, M. E.; Newport, R. J. Synthesis and Structural Characterization of P2O5-CaO- Na2O Sol-Gel Materials. **2007**, *353*, 1141–1149.

(17) Kokubo, T.; Takadama, H. How Useful Is SBF in Predicting in Vivo Bone Bioactivity? *Biomaterials* **2006**, *27* (15), 2907–2915. https://doi.org/10.1016/j.biomaterials.2006.01.017.

(18) Yan, X.; Yu, C.; Zhou, X.; Tang, J.; Zhao, D. Highly Ordered Mesoporous Bioactive Glasses with Superior in Vitro Bone-Forming Bioactivities. *Angew. Chemie - Int. Ed.* **2004**, *43*, 5980–5984. https://doi.org/10.1002/anie.200460598.

(19) Shi, Q. H.; Wang, J. F.; Zhang, J. P.; Fan, J.; Stucky, G. D. Rapid-Setting, Mesoporous, Bioactive Glass Cements That Induce Accelerated In Vitro Apatite Formation. *Adv. Mater.* **2006**, *18* (8), 1038–1042. https://doi.org/10.1002/adma.200502292.

(20) Knowles, J. C. Phosphate Based Glasses for Biomedical Applications. *J. Mater. Chem.* **2003**, *13* (10), 2395. https://doi.org/10.1039/b307119g.

(21) Vallet-Regí, M.; Colilla, M.; Izquierdo-Barba, I.; Manzano, M. Mesoporous Silica Nanoparticles for Drug Delivery: Current Insights. *Molecules* **2017**, *23* (1), 47. https://doi.org/10.3390/molecules23010047.

(22) Gounani, Z.; Asadollahi, M. A.; Pedersen, J. N.; Lyngsø, J.; Skov Pedersen, J.; Arpanaei, A.; Meyer, R. L. Mesoporous Silica Nanoparticles Carrying Multiple Antibiotics Provide Enhanced Synergistic Effect and Improved Biocompatibility. *Colloids Surfaces B Biointerfaces* **2019**, *175*, 498–508. https://doi.org/10.1016/j.colsurfb.2018.12.035.

(23) Jiang, S.; Zhang, Y.; Shu, Y.; Wu, Z.; Cao, W.; Huang, W. Amino-Functionalized Mesoporous Bioactive Glass for Drug Delivery. *Biomed. Mater.* **2017**, *12* (2), 25017. https://doi.org/10.1088/1748-605x/aa645d.

(24) Song, S.-W.; Hidajat, K.; Kawi, S. Functionalized SBA-15 Materials as Carriers for Controlled Drug Delivery: Influence of Surface Properties on Matrix−Drug Interactions. *Langmuir* **2005**, *21* (21), 9568–9575. https://doi.org/10.1021/la051167e.

(25) Rivadeneira, J.; Luz, G. M.; Audisio, M. C.; Mano, J. F.; Alejandro, A. Novel Antibacterial Bioactive Glass Nanocomposite Functionalized with Tetracycline Hydrochloride. **2015**, 128–135. https://doi.org/10.1515/bglass-2015-0012.

(26) Massiot, D.; Fayon, F.; Capron, M.; King, I.; Le Calvé, S.; Alonso, B.; Durand, J.-O.; Bujoli, B.; Gan, Z.; Hoatson, G. Modelling One- and Two-Dimensional Solid-State NMR Spectra. *Magn. Reson. Chem.* **2002**, *40* (1), 70–76. https://doi.org/10.1002/mrc.984.

(27) Kokubo, T.; Kushitani, H.; Sakka, S.; Kitsugi, T.; Yamamuro, T. Solutions Able to Reproduce in Vivo Surface-Structure Changes in Bioactive Glass-Ceramic A-W3. *J. Biomed. Mater. Res.* **1990**, *24* (6), 721–734. https://doi.org/10.1002/jbm.820240607.

(28) Al Qaysi, M.; Walters, N. J.; Foroutan, F.; Owens, G. J.; Kim, H. W.; Shah, R.; Knowles, J. C. Strontium- and Calcium-Containing, Titanium-Stabilised Phosphate-Based Glasses with Prolonged Degradation for Orthopaedic Tissue Engineering. *J. Biomater. Appl.* **2015**, *30* (3), 300–310.

(29) López-Noriega, A.; Arcos, D.; Izquierdo-Barba, I.; Sakamoto, Y.; Terasaki, O.; Vallet-Regí, M. Ordered Mesoporous Bioactive Glasses for Bone Tissue Regeneration. *Chem. Mater.* **2006**, *18* (13), 3137–3144. https://doi.org/10.1021/cm060488o.

(30) Zhang, F.; Yan, Y.; Yang, H.; Meng, Y.; Yu, C.; Tu, B.; Zhao, D. Understanding Effect of Wall Structure on the Hydrothermal Stability of Mesostructured Silica SBA-15. *J. Phys. Chem. B* **2005**, *109* (18), 8723–8732. https://doi.org/10.1021/jp044632+.

(31) Vinu, A. Two-Dimensional Hexagonally-Ordered Mesoporous Carbon Nitrides with Tunable Pore Diameter, Surface Area and Nitrogen Content. *Advanced functional*

materials. Wiley-VCH Verlag: Weinheim, Fed. Rep. of Germany : 2008, pp 816–827. https://doi.org/10.1002/adfm.200700783.

(32) Foroutan, F.; de Leeuw, N. H.; Martin, R. A.; Palmer, G.; Owens, G. J.; Kim, H. W.; Knowles, J. C. Novel Sol–Gel Preparation of $(P_2O_5)_{0.4}$–$(CaO)_{0.25}$–$(Na_2O)_X$–$(TiO_2)_{(0.35-X)}$Bioresorbable Glasses (X = 0.05, 0.1, and 0.15). *J. Sol-Gel Sci. Technol.* **2014**. https://doi.org/10.1007/s10971-014-3555-6.

(33) Foroutan, F.; Walters, N. J.; Owens, G. J.; Mordan, N. J.; Kim, H.-W.; de Leeuw, N. H.; Knowles, J. C. Sol-Gel Synthesis of Quaternary $(P_2O_5)_{55}$-$(CaO)_{25}$-$(Na_2O)_{(20-x)}$-$(TiO_2)_x$ Bioresorbable Glasses for Bone Tissue Engineering Applications (x = 0, 5, 10, or 15). *Biomed. Mater.* **2015**. https://doi.org/10.1088/1748-6041/10/4/045025.

(34) Abou Neel, E. A.; Knowles, J. C. Physical and Biocompatibility Studies of Novel Titanium Dioxide Doped Phosphate-Based Glasses for Bone Tissue Engineering Applications. *J. Mater. Sci. Mater. Med.* **2008**, *19* (1), 377–386.

(35) Eliaz, N.; Metoki, N. Calcium Phosphate Bioceramics : A Review of Their History, Structure, Properties, Coating Technologies and Biomedical Applications. *Materials (Basel)*. **2017**, *10* (334), 2–104. https://doi.org/10.3390/ma10040334.

(36) Durgalakshmi, D.; Rakkesh, R. A.; Balakumar, S. Stacked Bioglass/TiO_2 Nanocoatings on Titanium Substrate for Enhanced Osseointegration and Its Electrochemical Corrosion Studies. *Appl. Surf. Sci.* **2015**, *349*, 561–569. https://doi.org/10.1016/j.apsusc.2015.04.142.

(37) Cheng, N.; Wang, Y.; Zhang, Y.; Shi, B. The Osteogenic Potential of Mesoporous Bioglasses / Silk and Non-Mesoporous Bioglasses / Silk Scaffolds in Ovariectomized Rats : In Vitro and In Vivo Evaluation. *PLoS One* **2013**, *8* (11), 1–16. https://doi.org/10.1371/journal.pone.0081014.

(38) Coelho, C. C.; Grenho, L.; Gomes, P. S.; Quadros, P. A.; Fernandes, M. H. Nano-

Hydroxyapatite in Oral Care Cosmetics: Characterization and Cytotoxicity Assessment. *Sci. Rep.* **2019**, *9* (1), 11050. https://doi.org/10.1038/s41598-019-47491-z.

(39) Rana, K. S.; Souza, L. P. De; Isaacs, M. A.; Raja, F. N. S.; Morrell, A. P.; Martin, R. A. Development and Characterization of Gallium-Doped Bioactive Glasses for Potential Bone Cancer Applications. *ACS Biomater. Sci. Eng.* **2017**, *3* (12), 3425–3432. https://doi.org/10.1021/acsbiomaterials.7b00283.

(40) Xia, W.; Chang, J. Well-Ordered Mesoporous Bioactive Glasses (MBG): A Promising Bioactive Drug Delivery System. *J. Control. Release* **2006**, *110* (3), 522–530. https://doi.org/10.1016/j.jconrel.2005.11.002.

(41) Zhao, L.; Yan, X.; Zhou, X.; Zhou, L.; Wang, H.; Tang, J.; Yu, C. Mesoporous Bioactive Glasses for Controlled Drug Release. *Microporous Mesoporous Mater.* **2008**, *109* (1), 210–215. https://doi.org/10.1016/j.micromeso.2007.04.041.

For Table of Contents Use Only

Mesoporous phosphate-based glasses prepared via sol-gel

Farzad Foroutan, Benjamin A. Kyffin, Isaac Abrahams, Anna Corrias, Priyanka Gupta, Eirini Velliou, Jonathan C. Knowles, Daniela Carta

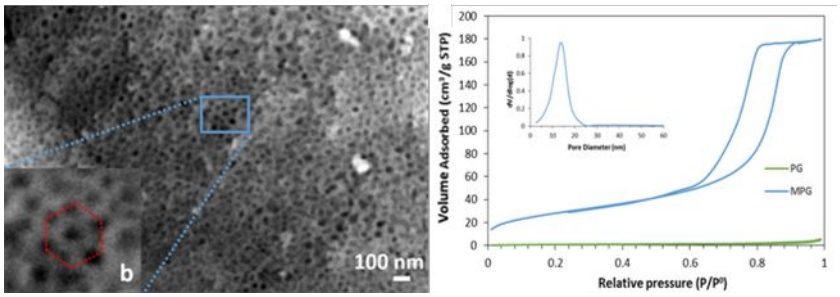

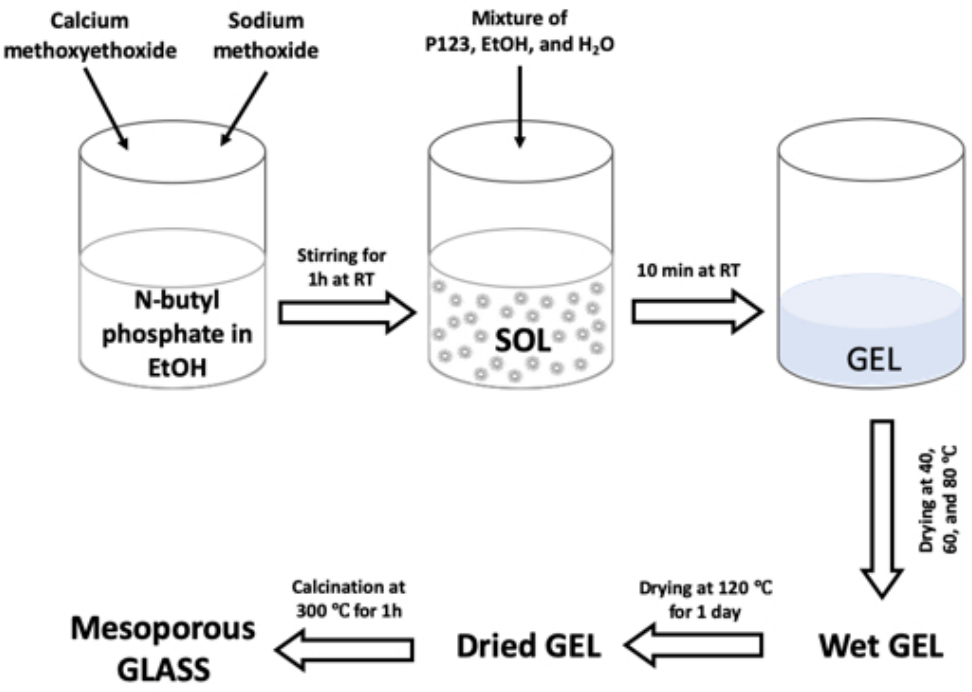

Figure 1. Flow diagram for the preparation of MPG.

139x99mm (96 x 96 DPI)

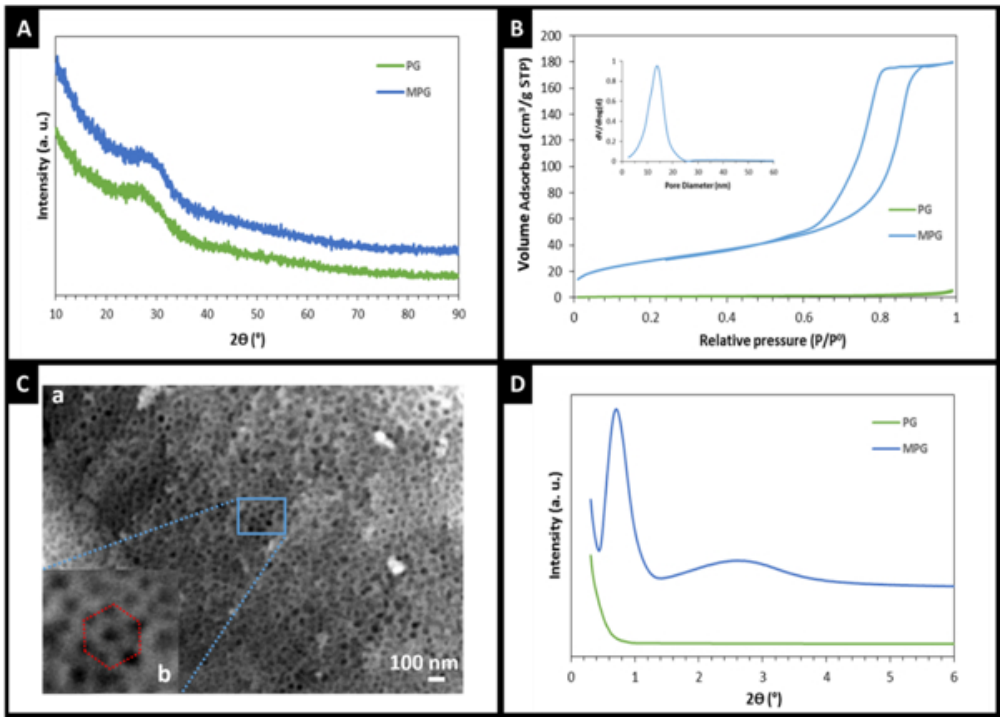

Figure 2. Characterisation of MPG and PG samples: (A) WA-XRD patterns, (B) N2 adsorption and desorption isotherms; inset: BJH pore size distribution, (C) SEM image of MPG (a); detail of blue squared area (b), and (D) LA-XRD patterns.

159x113mm (96 x 96 DPI)

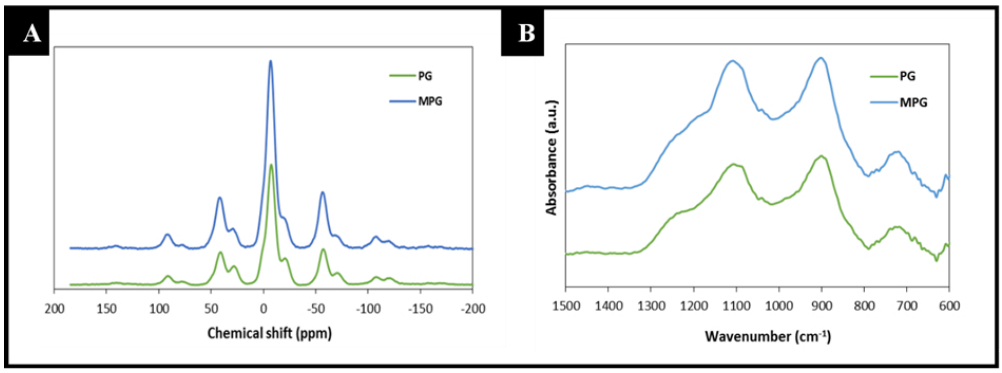

Figure 3. (A) 31P MAS NMR and (B) FT-IR spectra of MPG and PG samples.

250x91mm (96 x 96 DPI)

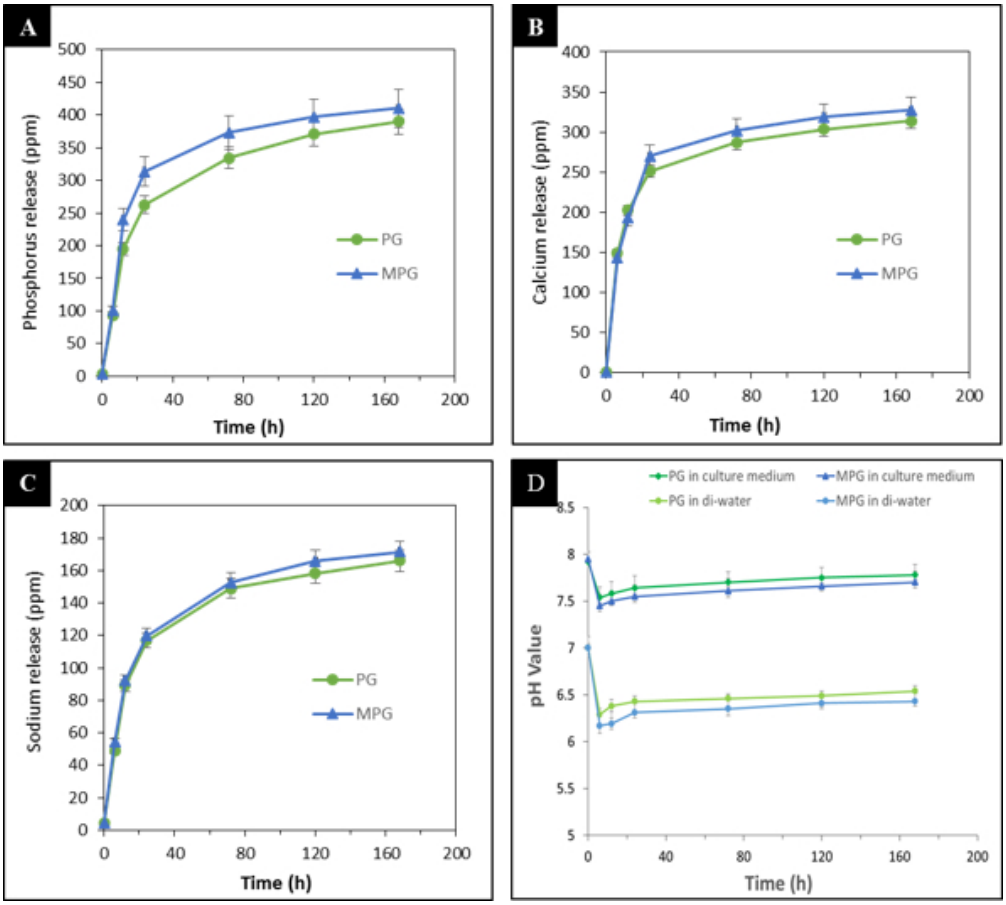

Figure 4. Release of (A) phosphorus, (B) calcium, and (C) sodium in deionised water measured by ICP-OES and (D) pH change in deionised water and cell culture medium as a function of time for MPG and PG samples.

156x140mm (96 x 96 DPI)

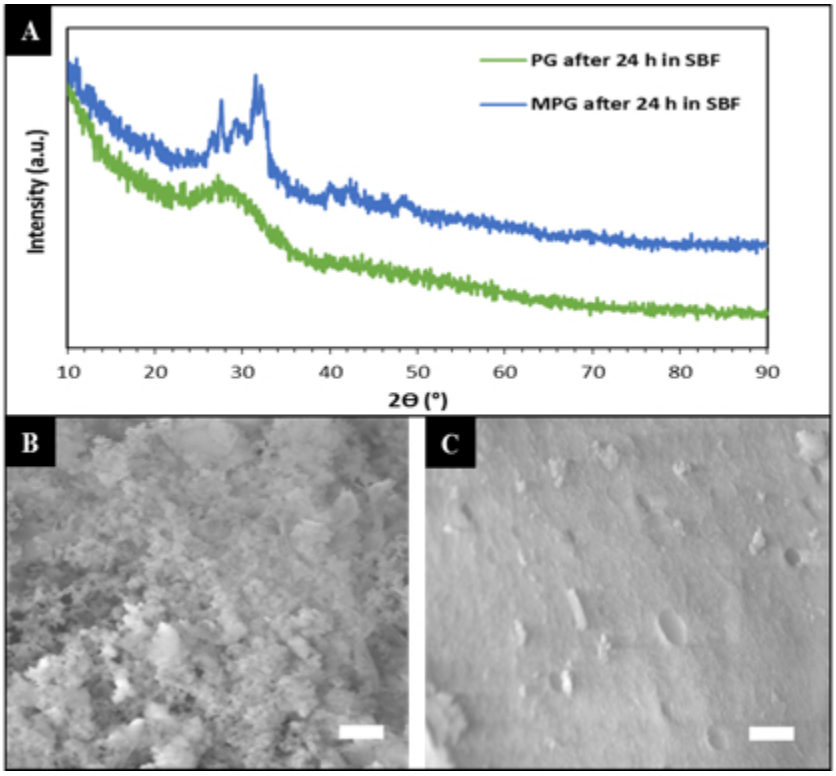

Figure 5. (A) XRD patterns of MPG and PG; SEM images of (B) MPG and (C) PG after immersion in SBF for 24 h at 37 °C. The scale bar is 1 μm.

110x101mm (96 x 96 DPI)

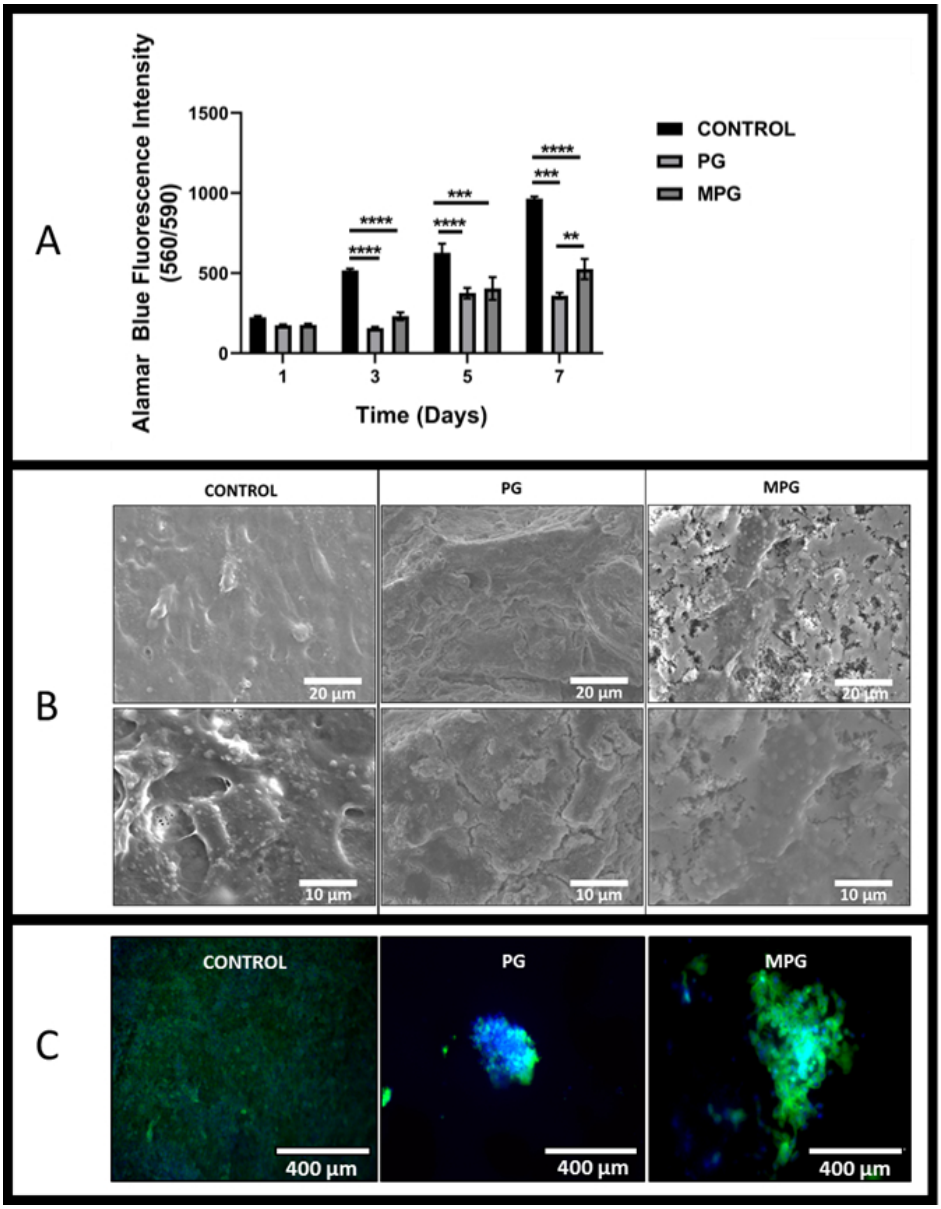

Figure 6. (A) Saos-2 cell viability measurement using the Alamar Blue fluorescence assay after 1, 3, 5 and 7 days; error bars are SD (n = 3); (B) SEM images showing Saos-2 cells attachment after 7 days at two different magnifications; (C) DAPI- Phalloidin staining after 7 days for the MPG and PG samples.

177x227mm (96 x 96 DPI)

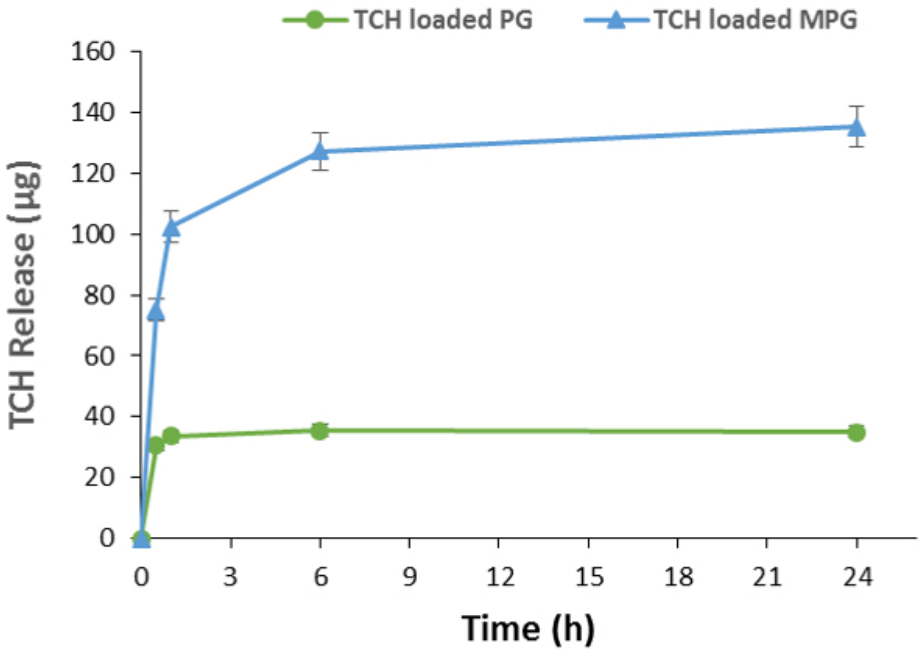

Figure 7. Release profiles of TCH as a function of time from loaded MPG and PG samples.

169x114mm (96 x 96 DPI)

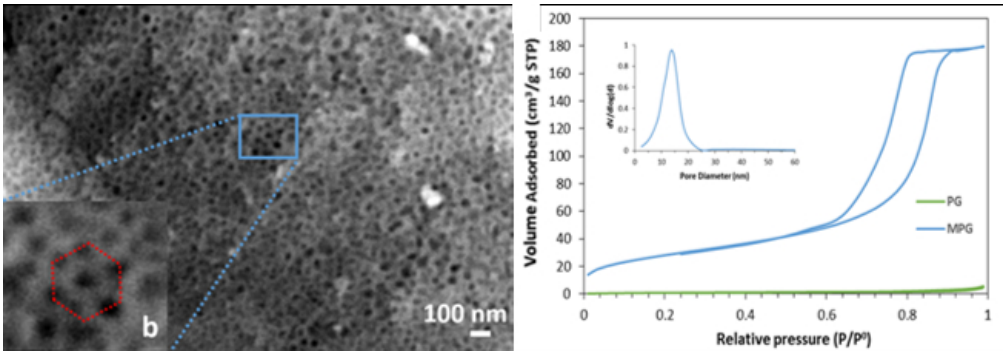

TOC

110x38mm (150 x 150 DPI)